Supporting Information

Enhanced visible-light-driven photocatalytic H_2 production and Cr(VI) reduction of a $ZnIn_2S_4/MoS_2$ heterojunction synthesized by the biomolecule-assisted microwave heating method

Watcharapong Pudkon[a], Hasliza Bahruji[b], Peter J. Miedziak[b,c], Thomas E. Davies[b], David J. Morgan[b], Samuel Pattisson[b], Sulawan Kaowphong[a,d,e,*], Graham J. Hutchings[b,*]

[a] *Department of Chemistry, Faculty of Science, Chiang Mai University, Chiang Mai 50200, Thailand*

[b] *Cardiff Catalysis Institute, School of Chemistry, Cardiff University, Main Building, Park Place CF10 3AT, Cardiff, UK*

[c] *School of Applied Sciences, University of South Wales, Pontypridd CF37 4AT, UK*

[d] *Environmental Science Research Center (ESRC), Faculty of Science, , Chiang Mai University, Chiang Mai 50200, Thailand*

[e] *Center of Excellence for Innovation in Chemistry, Faculty of Science, Chiang Mai University, Chiang Mai 50200, Thailand*

1. Calculation method for the apparent quantum yield (AQY)

The apparent quantum yield (AQY) of $ZnIn_2S_4$ and $ZnIn_2S_4/MoS_2$-40%wt photocatalysts for the H_2 production and Cr(VI) production were calculated according to the following equations:

$$\mathrm{AQY}(\%) = \frac{2 \text{ x number of evolved } \mathrm{H_2} \text{ molecules}}{\text{number of incident photon}} \times 100$$

where the light intensity is 119.43 mW/cm^2 and the irradiated surface area is 12.56 cm^2 with a 400 nm band pass filter.

$$\mathrm{AQY}(\%) = \frac{3 \text{ x number of reduced Cr(VI) ions}}{\text{number of incident photon}} \times 100$$

where the light intensity is 62.20 mW/cm^2 and the irradiated surface area is 6.25 cm^2 with a 400 nm band pass filter.

2. The procedure of the silver photo-deposition experiment

First, the $ZnIn_2S_4/MoS_2$-40%wt composite (50 mg, 150 mL) was dispersed in the $Ag(NO_3)_2$ solution (1 mM) under visible light irradiation for 360 min. Then, the photocatalyst after photo-depositing Ag was collected, washed several times with DI water and dried (60 ^oC).

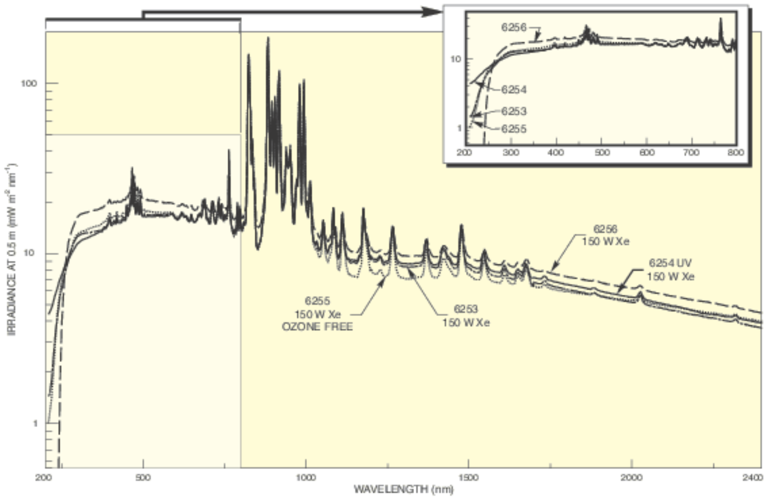

Fig. S1. Spectral irradiance of the 150 W Xe lamp (Model 6256, Newport[1,2]).

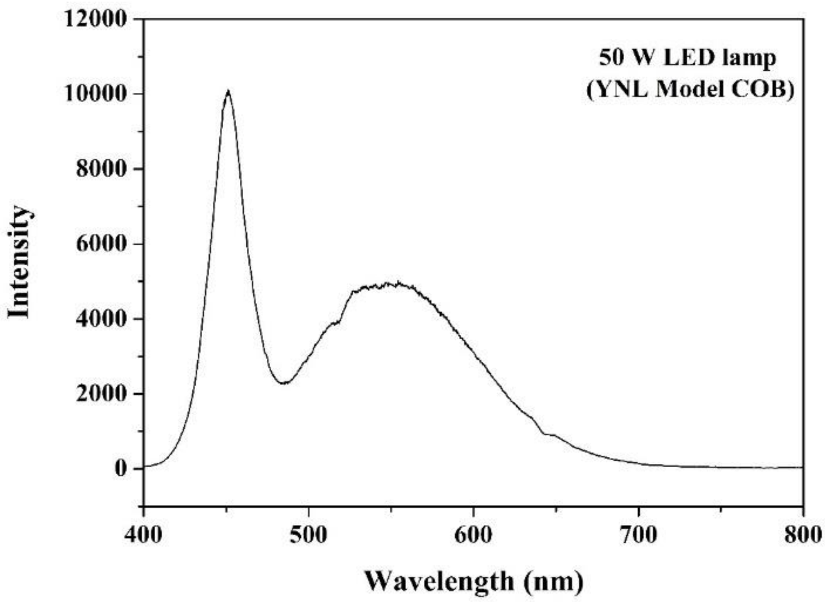

Fig. S2. Spectral irradiance of the 50 W LED lamp (YNL Model COB).

[1] https://www.newport.com.cn/medias/sys_master/images/images/hfb/hdf/8797196451870/Light-Sources.pdf

[2] https://www.newport.com.cn/n/information-on-spectral-irradiance-data

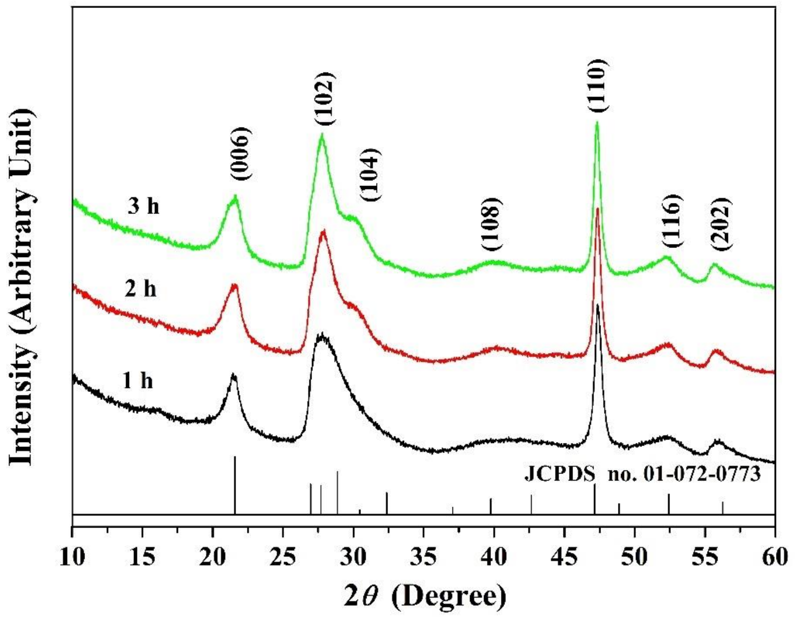

Fig. S3. XRD patterns of the $ZnIn_2S_4$ powders synthesized at different microwave heating times.

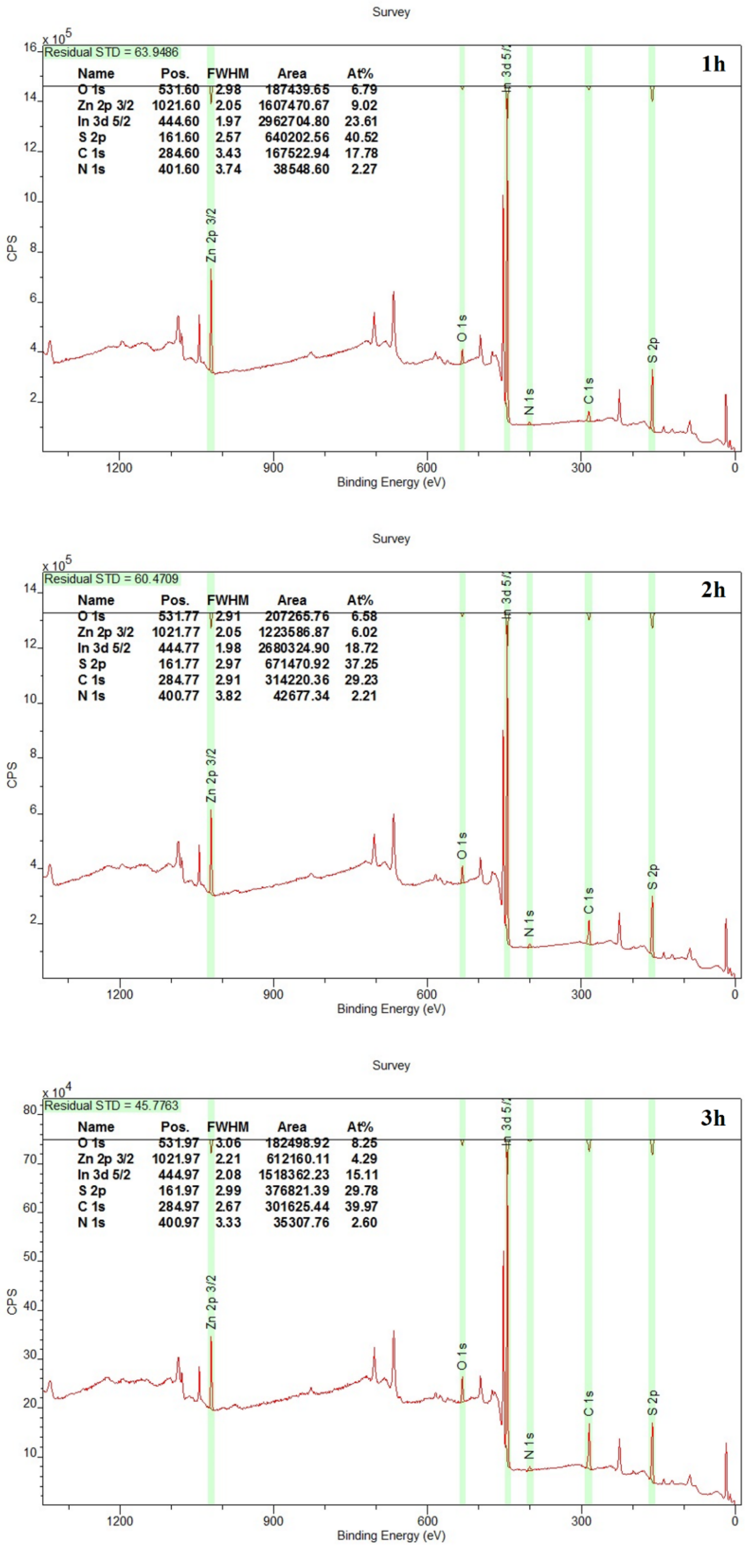

Fig. S4. Survey XPS spectra and the detailed chemical compositions of $ZnIn_2S_4$ synthesized at microwave heating time of 1, 2 and 3 h.

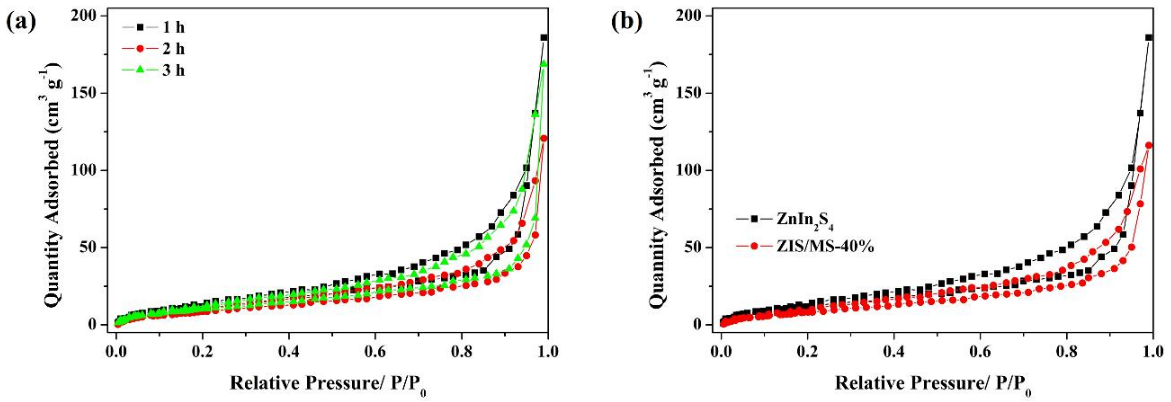

Fig. S5. The N_2 adsorption-desorption isotherms of **(a)** $ZnIn_2S_4$ synthesized at different microwave heating times, and **(b)** $ZnIn_2S_4/MoS_2$-40%wt compared with that of $ZnIn_2S_4$. All amples exhibit type-IV isotherms with the hysteresis loops in the range of 0.4-1.0 P/P_0, indicating the presence of slit-like mesopores due to the stacking of sheets.[3]

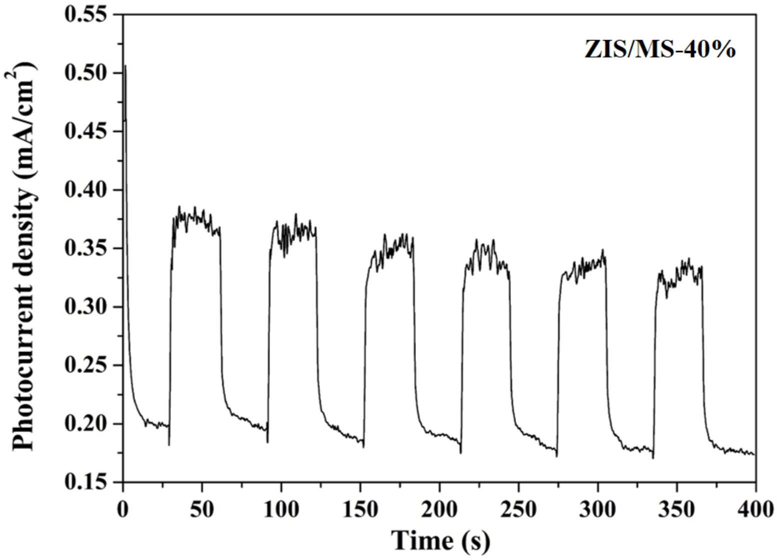

Fig. S6. Transient photocurrent density-time curve of the $ZnIn_2S_4/MoS_2$-40%wt photoelectrode.

[3] C.Liu, B. Chai, C. Wang, J. Yan, Z. Ren, Solvothermal fabrication of MoS_2 anchored on $ZnIn_2S_4$ microspheres with boosted photocatalytic hydrogen evolution activity, *Inter. J. Hydrogen Energy*, 2018, 43(14), 6977-6986.

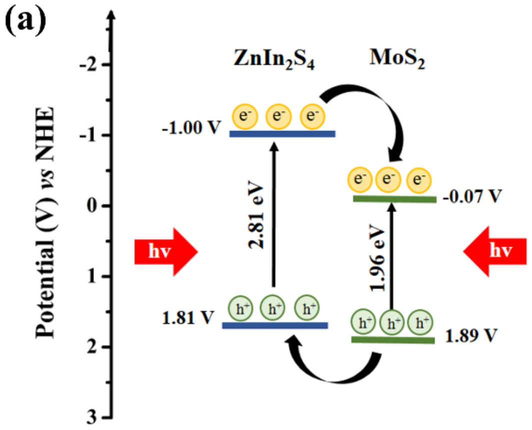

Fig. S7. The energy band positions and possible charges transfer in the $ZnIn_2S_4/MoS_2$ photocatalyst through **(a)** conventional type-II heterojunction and **(b)** Z-scheme heterojunction.

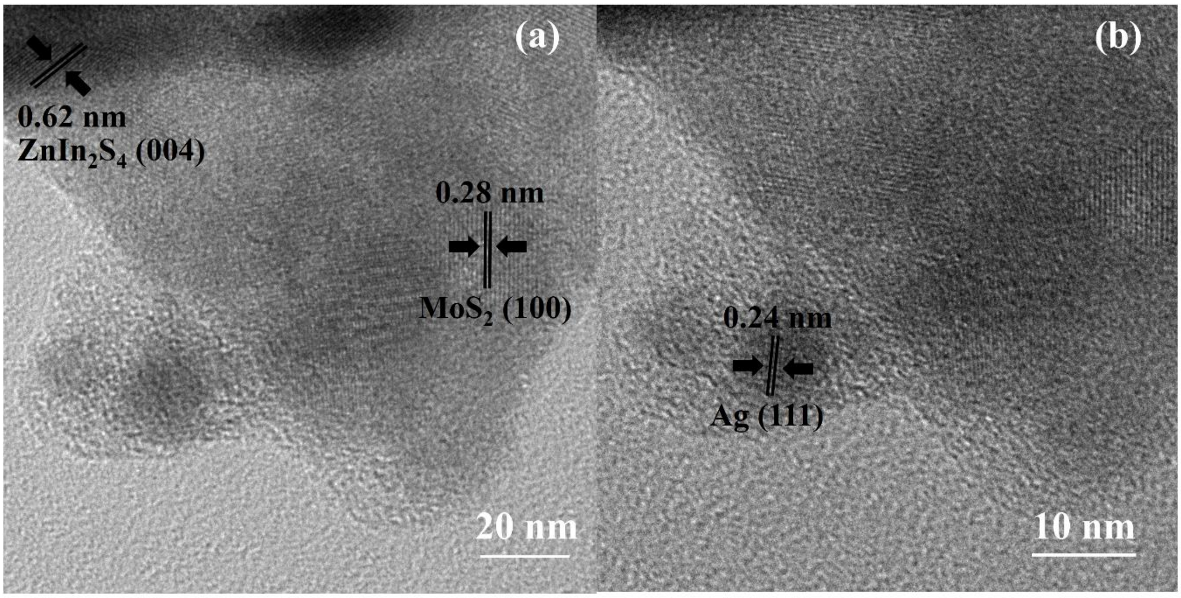

Fig. S8. (a)-(b) High-magnified TEM images of the silver nanoparticle deposited on the MoS_2 particle in the $ZnIn_2S_4/MoS_2$-40%wt composite. **(b)** Lattice fringe of Ag nanoparticles.

Table S1. Fitting parameter (χ^2), amplitudes (α_1, α_2), excited-state lifetime (τ_1, τ_2), and average exciton lifetime $<\tau>$ for $ZnIn_2S_4$ and $ZnIn_2S_4/MoS_2$-40%wt.

	χ^2	α_1	α_2	τ_1 (ns)	τ_2 (ns)	$<\tau>$ (ns)
$ZnIn_2S_4$	1.25	17.69	82.31	1.38	14.03	13.77
$ZnIn_2S_4/MoS_2$-40%wt	1.22	15.65	84.35	2.53	18.20	17.81

The average lifetime ($<\tau>$) was calculated using the equation[4,5]:

$<\tau> = (\alpha_1\tau_1^2 + \alpha_2\tau_2^2)/(\alpha_1\tau_1 + \alpha_2\tau_2)$

χ^2: the goodness of fit parameter. The ideal χ^2 values are 0.8-1.3.[6]

Table S2. The E_{VB} and E_{CB} of $ZnIn_2S_4$ and MoS_2 calculated by the Mulliken electronegativity (EN) theory and Mott-Schottky measurement.

Band Potential	Mulliken EN theory		Mott-Schottky plots	
	$ZnIn_2S_4$	MoS_2	$ZnIn_2S_4$	MoS_2
E_{VB}	1.71	1.84	1.81	1.89
E_{CB}	-1.10	-0.12	-1.00	-0.07

[4] C. Du, B. Yan, Z. Lin, G. Yang, Enhanced carrier separation and increased electron density in 2D heavily N-doped $ZnIn_2S_4$ for photocatalytic hydrogen production, *J. Mater. Chem. A*, 2020, **8**, 207.
[5] S. Manchala, V. S. R. K. Tandava, L. R. Nagappagari, S. M. Venkatakrishnan, D. Jampaiah, Y. M. Sabri, S. K. Bhargava, V. Shanker, Fabrication of a novel $ZnIn_2S_4$/g-C_3N_4/graphene ternary nanocomposite with enhanced charge separation for efficient photocatalytic H_2 evolution under solar light illumination, *Photochem. Photobiol.* Sci., 2019, 18, 2952
[6] D.F. Eaton, Recommended methods for fluorescence decay analysis, *Pure & Appl. Chem.*, 1990, **62(8)**, 1631-1648.

Table S3. Comparison of the photocatalytic H_2 production rates of the $ZnIn_2S_4/WS_2$ photocatalyst with the previous literature reports.

Photocatalyst	**Weight (mg)**	**Synthesis method**	**Light source details**	**Sacrificial reagent**	**H_2 production rate (μmol h^{-1} g^{-1})**
$ZnIn_2S_4/MoS_2$ (Our work)	100	Microwave heating method	150 W Xe lamp (λ > 400 nm)	Na_2S/Na_2SO_3	200.1
Ref. [23]	50	Hydrothermal method	300 W Xe lamp (λ > 420 nm)	Na_2S/Na_2SO_3	120
Ref. [7]	50	Impregnation method, followed by calcination	300 W Xe lamp (λ > 420 nm)	Na_2S/Na_2SO_3	306
Ref. [22]	80	Solvothermal method	300 W Xe lamp (λ > 420 nm)	Lactic acid	2,512.5
Ref. [21]	80	Solvothermal method	300 W Xe lamp (λ > 420 nm)	Na_2S/Na_2SO_3	3,891.6
Ref. [24]	80	Hydrothermal method	300 W Xe lamp (λ > 420 nm)	Lactic acid	4,287.5
Ref. [25]	100	Hydrothermal method	300 W Xe lamp (λ > 420 nm)	Lactic acid	8,047

References

[7] L. Wei, Y. Chen, Y. Lin, H. Wu, R. Yuan, Z. Li, *Appl. Catal. B.*, 2014, **144**, 521-527.

[21] Z. Zhang, L. Huang, J. Zhang, F. Wang, Y. Xie, X. Shang, Y. Gu, H. Zhao, X. Wang, *Appl. Catal. B.*, 2018, **233**, 112-119.

[22] C. Liu, B. Chai, C. Wang, J. Yan, Z. Ren, *Int. J. Hydrog. Energ.*, 2018, **43**, 6977-6986

[23] T. Huang, W. Chen, T. Y. Liu, Q. L. Hao, X. H. Liu, *Powder Tech.*, 2017, **315**, 157-162.

[24] B. Chai, C. Liu, C. Wang, J. Yan and Z. Ren, *Chinese J. Catal.*, 2017, **38**, 2067-2075.

[25] G. Chen, N, Ding, F. Li, Y. Fan, Y. Luo, D. Li, Q. Meng, *Appl. Catal. B.*, 2014, **160-161**, 614-620.

The difference in the H_2 production rate presented in Table S3 could be caused by the variation in the photocatalytic conditions such as the power of the light source and type/concentration of sacrificial reagents. [7,8,9] In addition, the characteristic of the photocatalysts that were synthesized via the different methods probably affects the H_2 production rate. For the hydrothermal process, $ZnIn_2S_4$ (or MoS_2) powder was firstly prepared and then being dispersed in the precursor for MoS_2 (or the solution of Zn^{2+}, In^{3+} and S^{2-}). Finally, the suspension was hydrothermally treated. This strategy could enable the nucleation process of the co-catalyst material on the host material's surface. As a result, the intimate construction of $ZnIn_2S_4/MoS_2$ heterostructure could be achieved, facilitating the interfacial charge transportation in the heterostructure. Although the activity of the $ZnIn_2S_4/MoS_2$ heterostructure prepared in this work is relative low, it exhibits the enhanced photocatalytic activity than that of $ZnIn_2S_4$ or MoS_2 for both H_2 production and Cr(VI) reduction reactions. Besides, the benefit of the proposed microwave heating synthesis is the reduction in the reaction time and energy consumption for the synthesis of photocatalytic materials.

[7] V. Kumaravel, M. D. Imam, A. Badreldin, R. K. Chava, J. Y. Do, M. Kang, A. Abdel-Wahab, Photocatalytic hydrogen production: role of sacrificial reagents on the activity of oxide, carbon, and sulfide catalysts, *Catalysts*, 2019, **9**, 276 (1-35).

[8] B. Weng, M. Qi, C. Han, Z. Tang, Y. Xu, Photocorrosion inhibition of semiconductor-based photocatalysts: basic principle, current development, and future perspective, *ACS Catalysis*, 2019, **9(5)**, 4642-4687.

[9] D. Zhang, J. Cheng, F. Shi, Z. Cheng, X. Yang, M. Cao, Low-temperature synthesis of ribbon-like orthorhombic $NaNbO_3$ fibers and their photocatalytic activities for H_2 evolution, *RSC Adv.*, 2015, **5**, 33001-33007.